1988

Chaotic particle transport in time-dependent Rayleigh-Benard convection

T. H. Solomon

Jerry P. Gollub
Haverford College

Repository Citation

"Chaotic Particle Transport in Rayleigh-Benard Convection," T.H. Solomon and J.P. Gollub, Phys. Rev. A 38, 6280 (1988).

Chaotic particle transport in time-dependent Rayleigh-Bénard convection

T. H. Solomon and J. P. Gollub

Department of Physics, Haverford College, Haverford, Pennsylvania 19041
and Department of Physics, University of Pennsylvania, Philadelphia, Pennsylvania 19104
(Received 9 June 1988)

The transport of passive impurities in nearly two-dimensional, time-periodic Rayleigh-Bénard convection is studied experimentally and numerically. The transport may be described as a one-dimensional diffusive process with a local effective diffusion constant $D^*(x)$ that is found to depend linearly on the local amplitude of the roll oscillation. The transport is independent of the molecular diffusion coefficient and is enhanced by 1–3 orders of magnitude over that for steady convective flows. The local amplitude of oscillation shows strong spatial variations, causing $D^*(x)$ to be highly nonuniform. Computer simulations of a simplified model show that the basic mechanism of transport is chaotic advection in the vicinity of oscillating roll boundaries. Numerical estimates of D^* are found to agree semiquantitatively with the experimental results. Chaotic advection is shown to provide a well-defined transition from the slow, diffusion-limited transport of time-independent cellular flows to the rapid transport of turbulent flows.

I. INTRODUCTION

Much can be learned from comprehensive studies of the transport of passive impurities in hydrodynamic flows. An understanding of transport phenomena is of practical importance in diverse fields of science and engineering including oceanography, astrophysics, biophysics, and chemical engineering. At a fundamental level, it is of interest to elucidate the various mechanisms that lead to transport enhancement as a fluid is driven farther from the motionless state. In addition, transport experiments can provide specific information about the dynamics of a flow that cannot be obtained easily from the velocity field alone. The reason for this surprising fact is that transport is affected by the trajectories of individual fluid elements, which can be quite complex[1] even in laminar flows. These trajectories are often sensitive to small amplitude instabilities. For this reason, transport experiments can be helpful in the studies of hydrodynamic instabilities.

Rayleigh-Bénard (RB) convection is a good model system for a comprehensive investigation of transport, since convective flows can be created ranging from time-independent, spatially periodic flows on the one hand, to turbulent flows on the other. As a result, the transport rates vary over a wide range. At one extreme, when the fluid is motionless, the transport is due entirely to molecular diffusion. At the other extreme (turbulent flows), transport is due to advection by the flow and is often described phenomenologically as enhanced (or "eddy") diffusion. We are not aware of studies of passive transport in turbulent RB convection; however, theoretical and experimental studies of similar systems have been reported.[2,3]

There are two important laminar flow regimes between these extremes: a time-independent and a time-periodic regime. In the time-independent regime, large-scale transport is limited by molecular diffusion between adjacent convection rolls. We presented an experimental study of this phenomenon in a previous article,[4] and it has also been discussed theoretically by various authors.[5-7] In the time-periodic regime, the transport is dominated by advection of tracer particles across roll boundaries. In this regime, particle trajectories may be *chaotic* (showing sensitivity to initial conditions). The differential equations for the velocity of a fluid element in a two-dimensional, time-dependent flow are formally those of a Hamiltonian system with two degrees of freedom. As a result, the particle trajectories display features of Hamiltonian chaos in real space. Chaotic structures such as heteroclinic tangles and invariant tori have been observed numerically and experimentally.[1,8-11] However, the quantitative effects of chaotic advection on transport have not been studied extensively.

In this paper, our previous experimental work on transport in steady RB convection is extended to the time-periodic, advection-dominated regime. Qualitative observations of the transport are presented, along with quantitative measurements of the transport rates as a function of the strength of the time dependence. A simplified numerical model is discussed,[12] in which transport between convection rolls is caused by chaotic advection due to lateral oscillations of the roll boundaries. The model gives a semiquantitative account of the experimental results. Finally, we give a general discussion of transport that should be applicable to a wider range of cellular flows.

II. EXPERIMENTAL METHODS

The convection cell used in these experiments is a rectangular box with horizontal dimensions 15 cm (along the x direction) by 1.5 cm (y direction) and a depth of 0.75 cm (z direction). The working fluid is water at an average temperature of 36 °C, where the Prandtl number is 4.7. Convection patterns are established with rolls oriented

parallel to the short side of the convection cell. Laser Doppler velocimetry (LDV) is used to characterize the flow and optical-absorption techniques are used to analyze the spreading of an injected impurity in the flow. Details of the experimental configuration can be found in the previous article.[4] Two impurities with different molecular diffusion coefficients are used: methylene blue, a molecular dye with diffusion coefficient $D_1 = 5.7 \times 10^{-6}$ cm^2/s; and a particulate impurity (vinyl toluene t-butylstyrene latex spheres) with diffusion coefficient $D_2 = 1.74 \times 10^{-8}$ cm^2/s.

The characterization of a velocity field with LDV techniques is straightforward for the time-independent case[4] but more problematic here due to the local nature of an LDV probe. To obtain spatial information about the flow it is necessary to collect velocity time series at numerous locations along the convection cell. The average value (time average) of the vertical velocity $\overline{v_z}$ at each location is then used to describe the spatial structure of the flow, and the standard deviation $\langle \sigma_v \rangle$ (averaged over a wavelength of the flow) is used as a measure of the local amplitude of time dependence.

After injection of an impurity, one-dimensional concentration profiles $c_1(x,t)$ are measured at the midheight of the cell by optical absorption. (The subscript is used to denote one-dimensional concentrations, integrated over y and z, with units of dye quantity per unit length.) An enhanced local-transport coefficient is defined using Fick's law for a coarse-grained (averaged over a convection roll) concentration profile $\overline{c}(x,t)$:

$$F(x,t) = D^*(x,t) \frac{\partial \overline{c}(x,t)}{\partial x} ,$$

where $F(x,t)$ is the flux of dye past the point x at time t and $\partial \overline{c}/\partial x$ is determined by measuring the slope of $c_1(x,t)$ between the centers of adjacent convection rolls. The enhanced diffusion coefficient $D^*(x,t)$ is determined by dividing $F(x,t)$ by $\partial \overline{c}/\partial x$. This local method has been tested on transport in time-independent convection.[4]

III. EXPERIMENTAL RESULTS

Transport experiments were performed at Rayleigh numbers R ranging from $R/R_c = 19$ (just above the onset of time dependence in this cell) through $R/R_c = 32$. (Here, R_c is the Rayleigh number corresponding to the onset of convection.) For each flow studied, LDV characterizations were obtained. An example of such a characterization is shown in Fig. 1, where the average value of the vertical component of velocity $\overline{v_z}$ and its standard deviation σ_v are plotted as a function of horizontal position x. Examination of this figure reveals a significant spontaneous, spatial nonuniformity in the flow. The wavelength of the convection pattern λ [distance between peaks in Fig. 1(a)] is somewhat larger near one end of the cell than elsewhere. Variations in wavelength up to 20% were noted in these experiments. The strength of the time dependence $\langle \sigma_v \rangle$ [the smooth curve in Fig. 1(b)] is also nonuniform and is apparently correlated with the variation in λ. Similar nonuniformities in the velocity field were observed in many (but not all) runs throughout
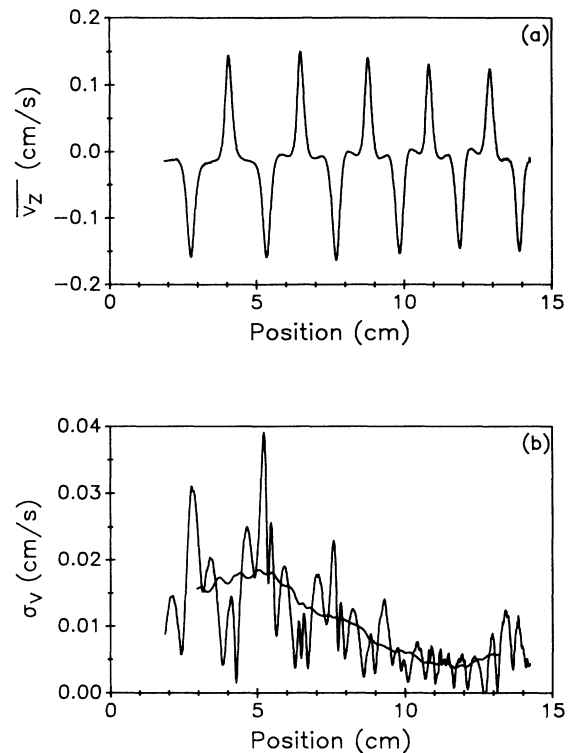

FIG. 1. LDV characterization of a time-periodic flow at $R/R_c = 26.1$. (a) Profile of the average vertical velocity $\overline{v_z}(x)$. (b) Standard deviation $\sigma_v(x)$ of the local velocity. The smooth curve is the spatially averaged standard deviation $\langle \sigma_v(x) \rangle$.

the range of Rayleigh numbers studied. It should be noted that both the magnitude of the spatial variations and the location of the maximum in $\langle \sigma_v \rangle$ change from run to run, implying that the effects are not due to irregularities in the construction or temperature control of the convection cell. Once a particular pattern is established, however, it is generally stable for at least a few days.

The oscillatory instabilty is accompanied by lateral oscillations of the roll boundaries. Figure 2 shows a time
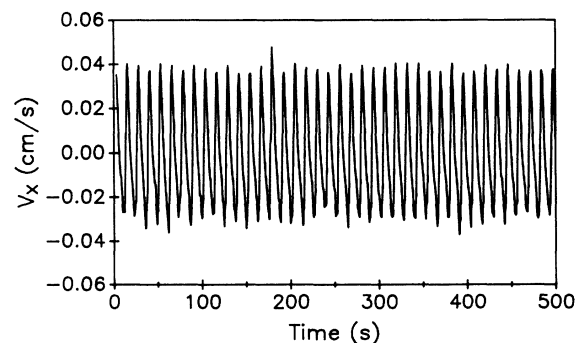

FIG. 2. Time series of the horizontal velocity near a roll boundary; $R/R_c = 26.1$. The oscillation between positive and negative velocities indicates lateral movement of the roll boundary.

series of horizontal velocity measurements taken in the vicinity of a roll boundary. The fact that the horizontal velocity oscillates between positive and negative values implies that the roll boundaries oscillate laterally, as expected of the "even" oscillatory instability.[13,14] The nature of the time dependence, however, is somewhat more complicated than this simple picture would suggest (see Sec. V).

Visual observation of the motion of an impurity injected through a small tube in the bottom corner of the cell clearly indicates the presence of advective transport between convection rolls. A photograph of this phenomenon is shown in Fig. 3. Small blobs of the impurity are pulled periodically from the corner of one roll into the next. Lines of impurity are stretched and folded repeatedly in the vicinity of the corners. Stretching and folding of this nature are common characteristics of horseshoe mappings in which a rectangle in phase space is stretched and folded onto itself. The presence of such mappings in a real space flow has been shown to be an indicator of chaotic advection.[9] Within the rolls, impurity concentrations are found to homogenize very rapidly (within a few minutes). This time is short compared to the typical time of approximately one-half day for the experiments.

Transport coefficients are measured for each run as a function of position and time. We find D^* to be independent of time, within the resolution of the data. [For each run, $D^*(x,t)$ is averaged over time and will be referred to as $D^*(x)$ from here on.] The spatial dependence of D^*, however, can be dramatic. A plot of $D^*(x)$ corresponding to the velocity profile of Fig. 1 is shown in Fig. 4. The spatial nonuniformities in $\langle \sigma_v(x) \rangle$ lead to variations in $D^*(x)$ by a factor of 10 from place to place. Variations in $D^*(x)$ are found whenever $\langle \sigma_v(x) \rangle$ is nonuniform, although the location of the maximum transport varies from run to run.
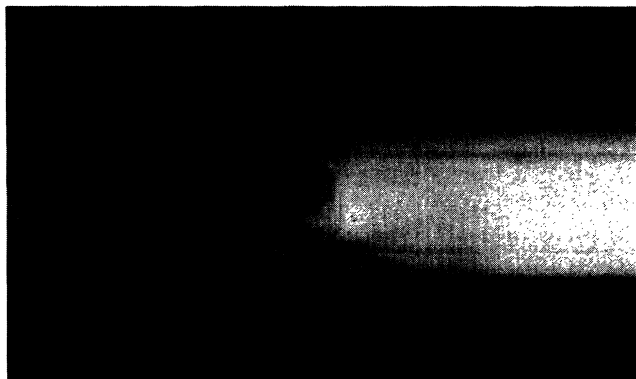

FIG. 3. Photograph of chaotic impurity transport $R/R_c=32$; latex sphere impurity. The photograph was taken less than 15 min after the start of the injection. The impurity is dark and has been injected from the left. (The first roll on the left is completely dark in this photo.) Note the pinching of blobs of impurity from the top-right corner of the first roll into the second. Also, note the folding of streaks of impurity across the bottom of the separatrix between the second and third rolls.
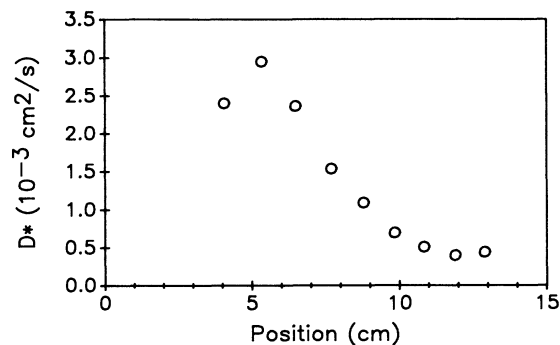

FIG. 4. Effective diffusion coefficient $D^*(x)$ for an experiment (same as in Fig. 1) at $R/R_c=26.1$ with methylene blue dye. Note the dramatic spatial nonuniformity in $D^*(x)$.

There is a monotonic relationship between D^* and $\langle \sigma_v \rangle$ which we determined experimentally. Because of the strong spatial variations often found in $D^*(x)$ and $\langle \sigma_v(x) \rangle$, it is not necessary to vary R to determine this relationship. We expect D^* to be proportional to λ^2 (see next section), so the data is rescaled to correspond to the critical wavelength λ_c for convection at $R \sim R_c$. Plots of $D^*(\lambda_c/\lambda)^2$ versus $\langle \sigma_v \rangle$ are shown in Fig. 5 for experiments conducted with both latex sphere and methylene
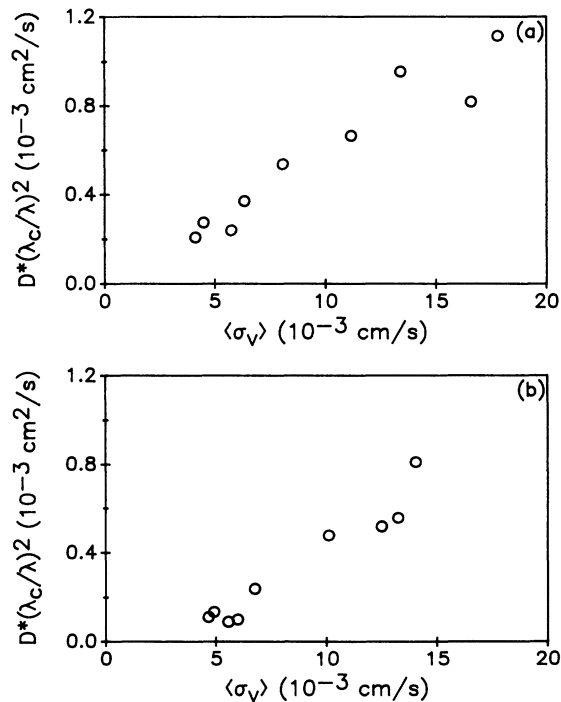

FIG. 5. Local transport enhancement as a function of the amplitude of local time dependence at $R/R_c=26.1$. The effective diffusion coefficient D^* has been scaled to the critical wavelength λ_c for convection near onset. Each figure contains data from a single run. (a) Methylene blue dye. (b) Latex sphere impurity.

blue impurities. An approximately linear relationship can be seen in both of these plots. Furthermore, the enhancement does not depend appreciably on the molecular diffusion coefficient of the impurity.

IV. NUMERICAL MODEL

In this section we describe a simplified model of transport in time-periodic RB convection that was briefly presented in a preliminary report.[12] A Lagrangian approach is taken in which the trajectories of individual impurity particles are obtained by integrating the equations describing the velocity field. The system is Hamiltonian: $\dot{x}(x,z,t)$ and $\dot{z}(x,z,t)$ are derived from a stream function

$$\Psi = \frac{A}{k}\sin\{k[x + B\sin(\omega t)]\}W(z) ,$$

where A is the maximum vertical velocity in the flow, k is the wave number $2\pi/\lambda$, and $W(z)$ is a function that satisfies the rigid boundary conditions at the top and bottom surfaces.[15] This stream function describes single-mode, two-dimensional convection with rigid boundary conditions. The term $B\sin\omega t$ represents the lateral oscillation of the roll pattern with amplitude B and frequency ω that is caused by the even oscillatory instability.[13]

Trajectories of particles near the separatrices are chaotic in this model.[12] Figure 6 shows the evolution of a line of tracer particles initially located along a separatrix. Qualitatively, the stretching and folding behavior observed in this figure is similar to that seen in the experiment (Fig. 3). More importantly, a quantitative comparison can be made between the model and the experimental transport data. Calculations of D^* as a function of B have been performed for the model. The parameters A and ω are set to match the conditions of the experiment. One convection roll is filled uniformly with 10 000 particles, and the trajectories of these particles are computed individually. After one complete period of oscillation, the number of particles that have been exchanged between adjacent rolls is counted to determine the net flux of impurity between rolls. An example of one of these simulations is shown in Fig. 7. Note the pinching of the impurity near the corner of the roll, similar to the pinching seen in Fig. 3. The calculated flux of impurity and the difference in concentration between the rolls is inserted into Fick's law to determine D^*. Values of D^* are determined numerically for amplitudes of oscillation B such that $0 < 2B/\lambda < 0.1$.

Knowledge of the dependence of D^* on λ and on the harmonic content of the velocity field is important for comparisons between the experimental and numerical data. A simple rescaling of the x variables in the velocity equations shows that the number of particles exchanged during one period of oscillation will not depend explicitly on λ. (This assertion was also tested numerically.) This information, along with Fick's law, predicts $D^* \sim \lambda^2$. The effect of the third harmonic in the velocity profile on the particle-exchange rate was also investigated. Simulations were performed with varying ratios of fundamental and third harmonic, holding the maximum vertical velocity constant. We found that the magnitude of the har-
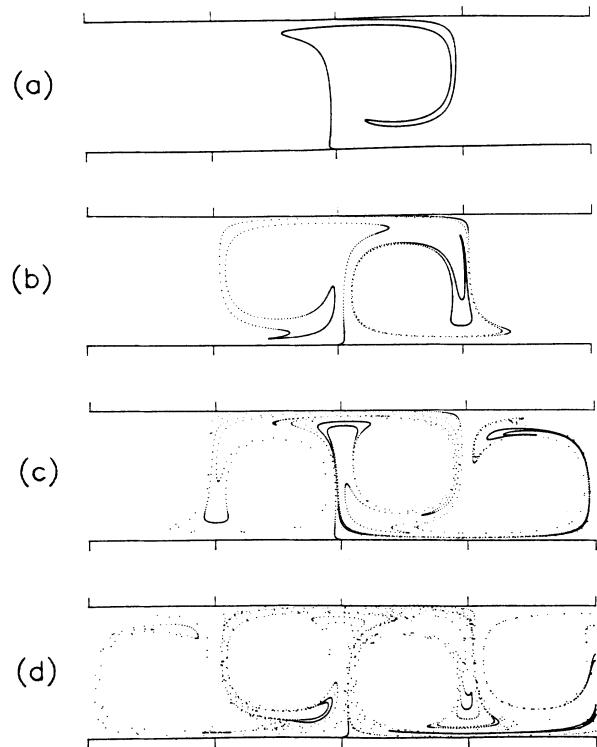

FIG. 6. Simulation of the evolution of a line of tracer particles, located initially along the separatrix between two convection rolls. The horizontal lines represent the upper and lower boundaries of the cell and the vertical marks denote roll boundaries. Parameters for this simulation: Amplitude $2B/\lambda = 0.12$, frequency $\omega = 0.49$ s^{-1}, velocity $A = 0.18$ cm/s. (a) Time $t = T/2$ (where $T = 2\pi/\omega$) is the period of oscillation), (b) $t = T$, (c) $t = 3T/2$, and (d) $t = 2T$.

monic content has a negligible effect on the rate of particle exchange.

For a proper comparison with the experimental data, the strength of the oscillation should be expressed in terms of $\langle \sigma_v \rangle$, not B. The conversion between B and $\langle \sigma_v \rangle$ is accomplished by expanding the $\dot{z}$ equation for
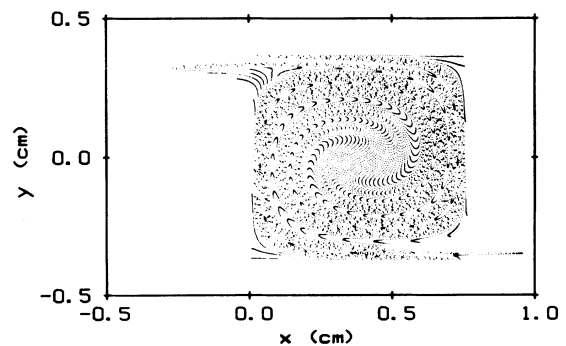

FIG. 7. Numerical determination of D^* by calculation of particle locations after one complete period of oscillation: $A = 0.14$ cm/s, $\omega = 0.49$ s^{-1}, $2B/\lambda = 0.02$. Note the pinching of impurity near the roll corners (similar to that observed in Fig. 3).
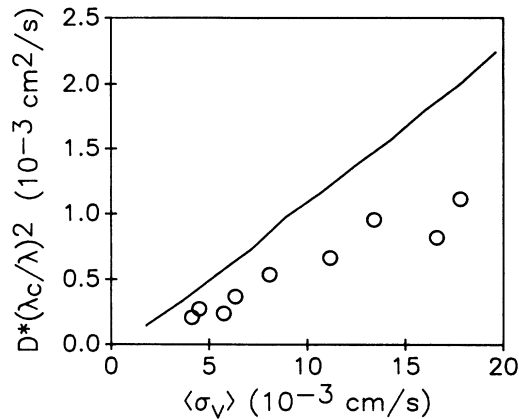
FIG. 8. Quantitative comparison between simulation (solid line) and experiment (open circles) for the effective transport coefficient. The experimental data is the same data shown in Fig. 5(a).

small B (corrected to include a term for the third harmonic), determining $\sigma_v(x,z)$ at $z=0$ and averaging over one complete wavelength of the roll pattern.

We find numerically that D^* depends linearly on B (and $\langle \sigma_v \rangle$) for small values of $2B/\lambda$ ($\lesssim 0.1$). A plot of D^* versus $\langle \sigma_v \rangle$ (for $\lambda=\lambda_c$) is shown in Fig. 8. The results of the numerical model are presented along with the experimental data from Fig. 5(a). For both the experimental and numerical data, D^* scales linearly with $\langle \sigma_v \rangle$. The slopes of the experimental and numerical data differ by about a factor of 2.

V. DISCUSSION

A. Comparison between model and experiment

Various factors must be considered in the comparison of the experimental and numerical results. First, the nature of the time dependence is somewhat more complicated than is implied by the model. It has been shown theoretically[14] that the first instability to time dependence in RB convection in fluids with Prandtl numbers $\gtrsim 2.5$ is not the "even" (transverse) oscillatory instability, but is, instead, a "hot-blob" instability, in which fluid elements hotter and colder than the surrounding fluid circulate within the convection rolls. There are two types of hot-blob instabilities, a one-blob instability (BE1) and a two-blob instability (BO2). The motions of the warm elements in adjacent rolls show reflection symmetry about the roll boundary. There is no lateral oscillation of the roll boundaries associated with a pure BE1 or BO2 oscillation, nor any contribution to advective transport between convection rolls.

We find that the roll boundaries do, in fact, oscillate laterally in the present experiments and that there is advective transport between rolls. However, the time dependence clearly is not due entirely to lateral oscillations, since plots of $\sigma_v(x)$ would then have local minima at the roll boundaries rather than maxima (Fig. 1). Shadow-

graph images (observed from the side) have been recorded to obtain qualitative information about the mechanisms causing the time dependence. In these images, hot and cold blobs are observed circulating within the rolls and, in addition, thermal boundaries between rolls are observed to oscillate laterally. Examples of these images are shown in Fig. 9. Figure 9(a) is an enhanced shadowgraph image in which three roll boundaries can be seen quite clearly. The presence of circulating warm and cold elements of fluid is emphasized in Fig. 9(b), which is an absolute value subtraction of two shadowgraph images separated in time by one-half oscillation period. The thermal boundary layers between rolls are not completely visible in Fig. 9(b), due to the subtraction process. Lateral motion of the roll boundaries can be seen quite clearly when the shadowgraph images are observed as a movie.

Evidently, the motion can be regarded as a superposition of lateral and BE1 oscillations. It is the lateral motion that is primarily responsible for the enhanced transport. Without detailed information about the contribution of a pure BE1 oscillation to the velocity field, *precise* quantitative estimates of the effects of the BE1 part of σ_v on the transport cannot be obtained numerically. Qualitatively, this part is not expected to contribute substantially to the transport. However, since it does influence σ_v, it may be responsible for much of the discrepancy between the experimental and numerical results in Fig. 8. Ideally, it would be desirable to make independent measurements of the relative strengths of the BE1 and even oscillations. This would enable us to isolate the effects of the even oscillations on the transport.

Other factors also affect the comparison between the numerical and experimental data, but are believed to be relatively minor. Quasiperiodic time dependence is observed occasionally in $v_z(t)$. However, this fact should
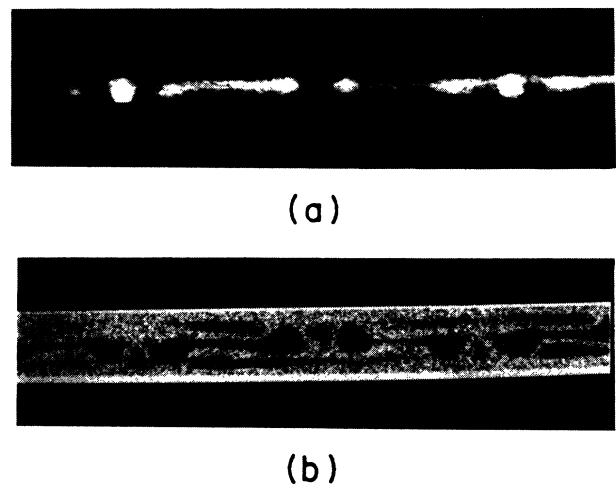

(a)

(b)

FIG. 9. (a) Shadowgraph image and (b) absolute value subtraction of two images separated time by one-half the period of oscillation at $R/R_c = 32$. (The convection cell is observed from the side and appears shallower than it actually is.) The motions of hot and cold fluid elements (dark spots in the image) can be seen clearly (b).

not cause significant error as the σ_v determined experimentally is proportional to the time average of the amplitude of the time dependence, and D^* depends linearly on this amplitude (according to the model). Another potential source of error is instrumental noise in the LDV system. We corrected for this approximately by subtracting the square of the instrumental noise from the square of the total standard deviation to obtain σ_v^2. However, it is likely that we have underestimated the noise (and hence may have overestimated σ_v). In addition, the experimental determination of $D^*(x)$ using Fick's law has a precision of about 10%. Finally, there are uncertainties of 10% in the estimation of the maximum vertical velocity of the flow and the frequency of the oscillation.

Though the numerical and experimental results shown in Fig. 8 differ quantitatively, they agree sufficiently well to support the basic mechanism assumed for the transport. Both the numerical and experimental transport coefficients scale linearly with the oscillation amplitude. (This linearity was previously predicted by Eckhardt.[16]) In addition, the absolute magnitudes of the enhancement differ only by a factor of 2, a discrepancy that is reasonable given the presence of the BE1 oscillation that does not contribute significantly to the transport but does contribute to $\langle \sigma_v \rangle$.

B. Spatial inhomogeneities and anomalous diffusion

The striking spatial nonuniformities in $\langle \sigma_v(x) \rangle$ and $D^*(x)$ observed in these experiments are indications of a symmetry-breaking instability similar to those observed in other experiments with RB convection.[17,18] The strength of time dependence $\langle \sigma_v \rangle$ is observed to grow with wavelength λ, implying that there is a causal link between the nonuniformities in these two quantities. It is natural to propose that variations in $\langle \sigma_v \rangle$ are caused by variations in λ, since convection is more unstable to the oscillatory instability at higher wavelengths.[13] However, nonuniformities in $\langle \sigma_v \rangle$ can also be observed when λ is held constant by external forcing.[18]

Anomalous diffusion (D^* explicitly dependent on time) has been predicted[16] for time-periodic RB convection. In an ideal two-dimensional flow, "classical barriers" to transport (invariant tori and cantori) would create nonuniformities in impurity concentrations within convection rolls. The diffusion of impurities across these barriers would impede large-scale transport and result in a time dependent D^*. These effects are expected to be significant only when concentrations within the rolls are nonuniform. In the present experiments, concentrations within the rolls are homogenized rapidly, eliminating the effects of anomalous diffusion. Various factors contribute to this homogenization. As shown in the previous paper,[4] molecular diffusion and advection due to a weak, three-dimensional, boundary-induced flow combine to mix impurities within rolls. This effect results in uniform concentrations within steady rolls for methylene blue dye but not for the more slowly diffusing particulate impurity. In time-periodic convection, on the other hand, even the particulate impurity is mixed rapidly within the rolls. This is an indication of mixing without classical barriers.

In a recent paper, Feingold et al.[19] show theoretically that certain classes of three-dimensional, time-periodic flows are susceptible to a process they term "singularity-induced diffusion" in which mixing is ergodic (there are no forbidden regions), even if the time dependence is infinitesimal. This process could possibly explain the rapid homogenization observed in these experiments.

C. General discussion of transport phenomena in cellular flows

Here we propose a general scheme for summarizing enhanced transport in cellular flows such as RB convection and Taylor-Couette flow. In Fig. 10 the enhanced diffusion coefficient D^* is plotted schematically as a function of a characteristic velocity of v of the flow for two different impurities. (We plot D^* versus v instead of using the dimensionless quantity R because transport is a kinematic phenomenon, dependent directly on the velocity of the fluid.) Various regimes are identified. Regime I denotes the zero-velocity regime, where D^* is equal to the molecular diffusion coefficient D of the impurity. (D_1 and D_2 refer to the molecular diffusion coefficients of methylene blue and 0.369 μm latex spheres, respectively.) Regime II denotes the diffusion-limited regime studied experimentally in the previous paper[4] and theoretically by various authors.[5−7] In this regime, D^* is proportional to $v^{1/2}$ and maintains its dependence on D. The time-periodic regime (III) of this paper is accompanied by an additional dramatic enhancement of several orders of magnitude (depending on the impurity used) due to chaotic advection. The dependence of the transport on D is eliminated in this regime. As a result, chaotic advec-
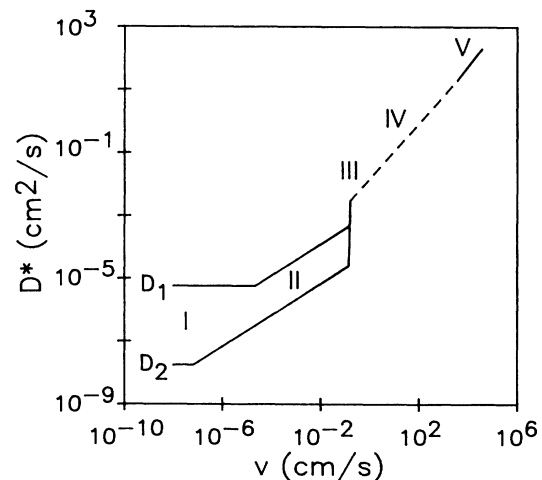

FIG. 10. Diagram of transport in convective flows, covering all the relevant regimes: I, molecular diffusion; II, diffusion-limited transport; III, chaotic advection (near the onset of time dependence); IV, chaotic but nonturbulent velocity field (not studied); V, turbulent transport (estimated, based on similar studies in other systems). D_1 and D_2 are the molecular diffusion coefficients of methylene blue and latex sphere impurities, respectively.

tion provides a well-defined transition between the slow transport of the diffusion-limited regimes and the rapid transport of the turbulent regime.

For the turbulent regime (V), we rely on theoretical[2] and experimental[3] studies in other systems for our estimates of D^*. Here, D^* is expected to be proportional to the rms velocity of the flow. The form of the curve in the region (IV) between chaotic advection and turbulent advection is speculative, since this regime has not been investigated in detail. This could be the goal of a future experiment. We suggest that the main features of Fig. 10 would apply qualitatively to Couette flow and other cellular flows as well.

[1]H. Aref, J. Fluid Mech. **143**, 1 (1984).
[2]Ya. B. Zeldovich, Dokl. Akad. Nauk SSSR **266**, 821 (1982) [Sov. Phys. Dokl. **27**, 797 (1982)].
[3]W. Y. Tam and H. L. Swinney, Phys. Rev. A **36**, 1374 (1987).
[4]T. H. Solomon and J. P. Gollub, Phys. Fluids **31**, 1372 (1988).
[5]B. Shraiman, Phys. Rev. A **36**, 261 (1987).
[6]P. McCarty and W. Horsthemke, Phys. Rev. A **37**, 2112 (1988).
[7]M. N. Rosenbluth, H. L. Berk, I. Doxas, and W. Horton, Phys. Fluids **30**, 2636 (1987).
[8]J. Chaiken, R. Chevray, M. Tabor, and Q. M. Tam, Proc. R. Soc. London Ser. A **408**, 165 (1987).
[9]W. L. Chien, H. Rising, and J. M. Ottino, J. Fluid Mech. **170**, 355 (1986).
[10]D. V. Khakhar, H. Rising, and J. M. Ottino, J. Fluid Mech. **172**, 419 (1986).
[11]J. M. Ottino, C. W. Leong, H. Rising, and P. D. Swanson, Nature **333**, 419 (1988).
[12]J. P. Gollub and T. H. Solomon, in *Proceedings of the Fritz Haber International Symposium*, edited by I. Procaccia (Plenum, New York, 1988).
[13]R. M. Clever and F. H. Busse, J. Fluid Mech. **65**, 625 (1974).
[14]E. W. Bolton, F. H. Busse, and R. M. Clever, J. Fluid Mech. **164**, 469 (1986).
[15]S. Chandresekhar, *Hydrodynamic and Hydromagnetic Stability* (Clarendon, Oxford, 1961), p. 39.
[16]B. Eckhardt (unpublished).
[17]S. Ciliberto and P. Bigazzi, Phys. Rev. Lett. **60**, 286 (1988).
[18]P. Bergé and M. Dubois (private communication).
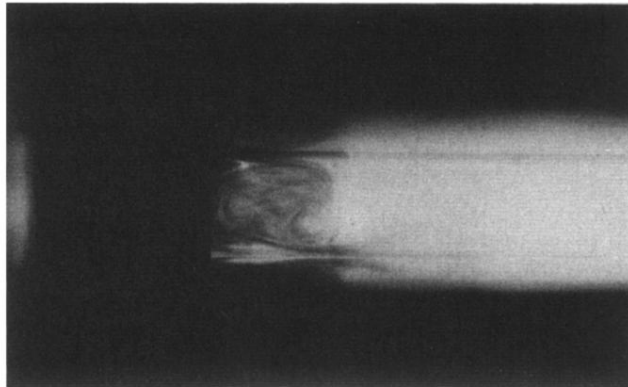[19]M. Feingold, L. Kadanoff, and O. Piro, J. Stat. Phys. **50**, 529 (1987).

FIG. 3. Photograph of chaotic impurity transport $R/R_c = 32$; latex sphere impurity. The photograph was taken less than 15 min after the start of the injection. The impurity is dark and has been injected from the left. (The first roll on the left is completely dark in this photo.) Note the pinching of blobs of impurity from the top-right corner of the first roll into the second. Also, note the folding of streaks of impurity across the bottom of the separatrix between the second and third rolls.
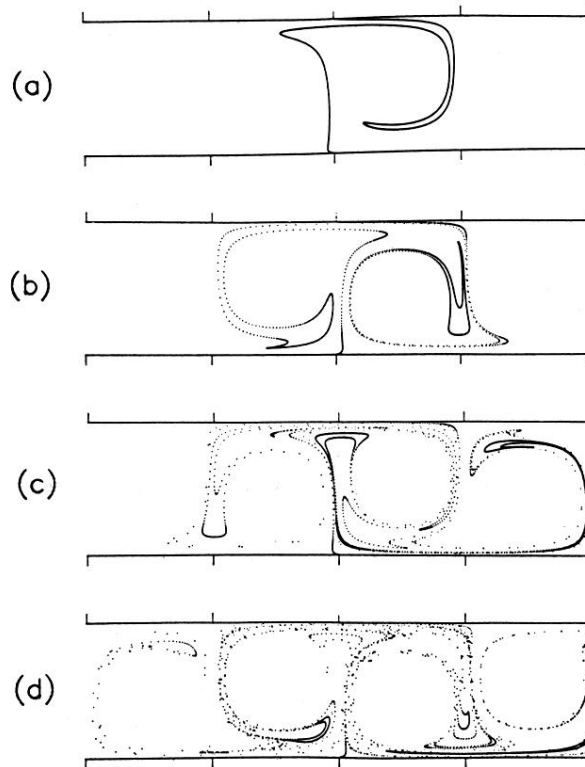
FIG. 6. Simulation of the evolution of a line of tracer particles, located initially along the separatrix between two convection rolls. The horizontal lines represent the upper and lower boundaries of the cell and the vertical marks denote roll boundaries. Parameters for this simulation: Amplitude $2B/\lambda = 0.12$, frequency $\omega = 0.49$ s^{-1}, velocity $A = 0.18$ cm/s. (a) Time $t = T/2$ (where $T = 2\pi/\omega$ is the period of oscillation), (b) $t = T$, (c) $t = 3T/2$, and (d) $t = 2T$.
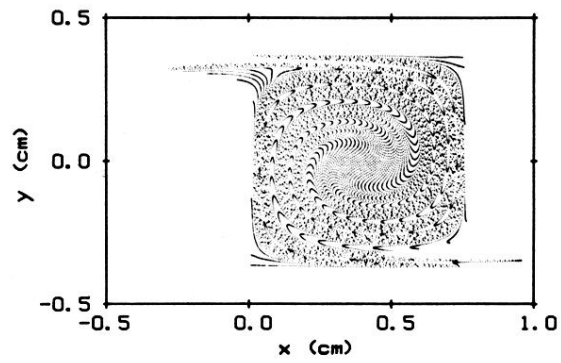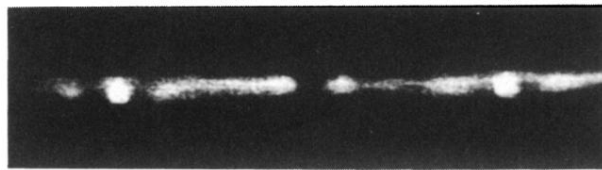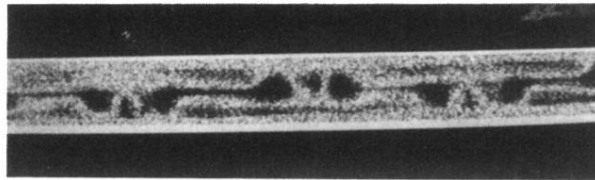
FIG. 7. Numerical determination of D^* by calculation of particle locations after one complete period of oscillation: $A=0.14$ cm/s, $\omega=0.49$ s^{-1}, $2B/\lambda=0.02$. Note the pinching of impurity near the roll corners (similar to that observed in Fig. 3).

(a)

(b)

FIG. 9. (a) Shadowgraph image and (b) absolute value subtraction of two images separated time by one-half the period of oscillation at $R/R_c = 32$. (The convection cell is observed from the side and appears shallower than it actually is.) The motions of hot and cold fluid elements (dark spots in the image) can be seen clearly (b).